

## Carrying the past to the future: Distinct brain networks underlie individual differences in human spatial working memory capacity



Siwei Liu<sup>a</sup>, Jia-Hou Poh<sup>a</sup>, Hui Li Koh<sup>a</sup>, Kwun Kei Ng<sup>a</sup>, Yng Miin Loke<sup>a</sup>, Joseph Kai Wei Lim<sup>a</sup>, Joanna Su Xian Chong<sup>a</sup>, Juan Zhou<sup>a,b,\*</sup>

<sup>a</sup> Center for Cognitive Neuroscience, Neuroscience and Behavioral Disorders Program, Duke-NUS Medical School, National University of Singapore, Singapore

<sup>b</sup> Clinical Imaging Research Centre, The Agency for Science, Technology and Research and National University of Singapore, Singapore

### ARTICLE INFO

#### Keywords:

Spatial working memory  
EEG-fMRI  
Individual difference  
Negative slow wave  
Fronto-parietal network  
Default mode network

### ABSTRACT

Spatial working memory (SWM) relies on the interplay of anatomically separated and interconnected large-scale brain networks. EEG studies often observe load-associated sustained negative activity during SWM retention. Yet, whether and how such sustained negative activity in retention relates to network-specific functional activation/deactivation and relates to individual differences in SWM capacity remain to be elucidated. To cover these gaps, we recorded concurrent EEG-fMRI data in 70 healthy young adults during the Sternberg delayed-match-to-sample SWM task with three memory load levels. To a subset of participants ( $N = 28$ ) that performed the task properly and had artefact-free fMRI and EEG data, we employed a novel temporo-spatial principal component analysis to derive load-dependent negative slow wave (NSW) from retention-related event-related potentials. The associations between NSW responses with SWM capacity were divergent in the higher ( $N = 14$ ) and lower ( $N = 14$ ) SWM capacity groups. Specifically, larger load-related increase in NSW amplitude was associated with greater SWM capacity for the higher capacity group but lower SWM capacity for the lower capacity group. Furthermore, for the higher capacity group, larger NSW amplitude was related to greater activation in bilateral parietal areas of the fronto-parietal network (FPN) and greater deactivation in medial frontal gyrus and posterior mid-cingulate cortex of the default mode network (DMN) during retention. In contrast, the lower capacity group did not show similar pattern. Instead, greater NSW was linked to higher deactivation in right posterior middle temporal gyrus. Our findings shed light on the possible differential EEG-informed neural network mechanism during memory maintenance underlying individual differences in SWM capacity.

### Introduction

Working memory capacity is an important building block in normal cognitive functions (Constantinidis and Klingberg, 2016). It is thus not surprising that working memory capacity underlies individual differences in normal cognitive development (Kane and Engle, 2002) and disease-related changes (Luck and Vogel, 2013; Park and Holzman, 1992). More specifically, individual differences in holding spatial information in an active state for seconds, named spatial working memory (SWM) capacity, have been documented. Often reflected in difference in brain activities, individual differences in SWM capacity were related to development of arithmetic cognition (Ashkenazi et al., 2013), widened

among the elderly (Nagel et al., 2009), hindered cognitive declines in normal ageing (Anguera et al., 2010), and pathological changes related to neuropsychiatric disorders (Fusar-Poli et al., 2010; Lenartowicz et al., 2014; Park and Holzman, 1992). Understanding the neural substrates supporting SWM capacity can hence shed light on the mechanisms behind individual differences in both normal development and disease-induced deviations.

Individual differences may stem from various phases of SWM processing including encoding, retention, and retrieval. Here we focused on the retention phase where the location of the stimulus could no longer be seen. EEG studies using the Sternberg delayed-match-to-sample SWM task (Sternberg, 1966) often observe sustained negative activity during

**Abbreviations:** NSW, negative slow wave; SWM, spatial working memory; PCA, principal component analysis; PC, principal component; FPN, fronto-parietal network; DMN, default mode network; Kmax, maximum Cowen's K; FS, factor score; MTG, middle temporal gyrus; LSPG, left superior parietal gyrus; rSPG, right superior parietal gyrus; PCC, posterior cingulate cortex; MCC, middle cingulate cortex; SMFG, superior medial frontal gyrus.

\* Corresponding author. Duke-NUS Medical School, 8 College Road, #06-15, 169857, Singapore.

E-mail address: [helen.zhou@duke-nus.edu.sg](mailto:helen.zhou@duke-nus.edu.sg) (J. Zhou).

<https://doi.org/10.1016/j.neuroimage.2018.04.014>

Received 19 June 2017; Received in revised form 7 March 2018; Accepted 8 April 2018

Available online 10 April 2018

1053-8119/© 2018 Elsevier Inc. All rights reserved.

retention, and this negative slow wave (NSW) was thought to be supported by neural synchrony between fronto-parietal and occipital regions (Palva et al., 2010). The amplitude of NSW can be modulated by SWM load, with a greater load inducing larger NSW during retention (Drew et al., 2006). Interestingly, this modulation of NSW amplitude is closely related to individual differences in SWM capacity, and working memory load exceeding individual capacity did not lead to further increase in the NSW amplitudes (Vogel and Machizawa, 2004). It is thus a useful measurement of individual differences in SWM capacities.

While EEG recordings contain valuable time-sensitive information, fMRI studies can also offer unique perspective (Jorge et al., 2014). Successful retention of the spatial information relies on cognitive components including selective attention and distractor inhibition (Gazzaley and Nobre, 2012; Unsworth et al., 2014). Previous task-based fMRI studies have suggested the involvement of both fronto-parietal network (FPN) and sensory cortices in supporting SWM, with the former relating to general executive control and higher working memory capacity (Linden et al., 2003; Rottschy et al., 2012; Todd and Marois, 2004) and the latter supporting the representations of the memoranda (Ku et al., 2015; Sreenivasan et al., 2014a, 2014b). Recent computational methods have also suggested that visual-spatial information can be reconstructed based on activity information in the FPN (Ester et al., 2015; Sprague et al., 2014). Particularly, reconstruction was successful for the remembered but not for the forgotten locations (Sprague et al., 2014). In addition to the FPN, the task-negative default mode network (DMN) has also been shown to be associated with working memory performance, exhibiting greater deactivation with greater working memory load (Gordon et al., 2012). The FPN and the DMN, referred to respectively as the task-positive and task-negative networks, have both been linked to individual differences in working memory capacity (Burzynska et al., 2011; Darki and Klingberg, 2015; Ekman et al., 2016; Gordon et al., 2012; Vermeij et al., 2014). Specifically, for a visual-spatial working memory task consisting of encoding, retention, and retrieval phases, the anti-correlation between the networks was most prominent during the retention phase (Piccoli et al., 2015). Additionally, modularity and integration of brain networks have been linked to working memory capacity (Alavash et al., 2015; Stevens et al., 2012). This further encouraged us to examine the neural responses during the retention phase in query of SWM individual differences, in which interaction of these brain networks may selectively maintain the memory presentation and suppress interference that potentially corrupts the memory (Gordon et al., 2012).

While EEG studies provide the time courses of the related brain responses, fMRI studies offer the spatial information of the relevant brain networks. Studies using concurrent recording of EEG and fMRI should thus shed light on how the brain temporally and spatially responds to spatial working memory loads. Thus far, such attempts were mostly from studies integrating fMRI with the frequency domain of the EEG (e.g., (Michels et al., 2012; Miller et al., 2008; Mizuhara et al., 2015; Sammer et al., 2007)), while integration of fMRI and event-related potential (ERP) tend to focus on the encoding and/or the retrieval phase (Galashan et al., 2015; Hoffmann et al., 2014; Marchand et al., 2006; Miller et al., 2008; Rawdon et al., 2013; Zhang et al., 2015). The former has identified different functions of gamma, theta and alpha band oscillations. The latter pointed to the importance of the attention effect (e.g., the reduced P3 in higher load (Zhang et al., 2015)). However, concurrent EEG-fMRI studies have yet to clarify the temporo-spatial properties of the brain responses in the retention phase. It remains to be investigated how EEG responses during retention phase are related to task-positive and task-negative brain networks.

To cover these gaps, we employed concurrent EEG-fMRI recording to examine both EEG NSW and blood-oxygen-level dependent (BOLD) responses during the Sternberg delayed-match-to-sample SWM task in healthy young adults. Using temporo-spatial principal component analysis (PCA), we sought to identify load-related NSW component during retention and examine its association with individual differences in SWM

capacity. Furthermore, we hypothesized that the NSW component would be related to BOLD activation in the FPN and sensory networks and deactivation in the DMN. Nevertheless, this association might vary depending on the SWM capacity.

## Methods

### Participants

Healthy young participants were recruited both within the National University of Singapore and community, based on the following requirements: (1) age between 18 and 35; (2) Chinese ethnicity; (3) right handed; (4) have no history of psychiatric or neurologic disorders; (5) not pregnant; (6) normal or corrected to normal vision (with non-coloured contact lenses); (7) no metallic objects in the body; (9) no long-term medications of antipsychotics, anxiolytics, anti-depressants; (10) no discomfort in a confined space. Ethics approval was obtained from the National University of Singapore Institutional Review Board (NUS-IRB). The study was conducted in accordance with the Declaration of Helsinki. Written informed consent was obtained. For participants below the age of 21, parental consent was also obtained.

We recorded concurrent EEG-fMRI data during the SWM task from 70 participants. Criterion for exclusion are as follows: (1) behavioural response accuracy in load 1 condition was lower than 85%; (2) EEG data did not fulfill quality requirements (see EEG data preprocessing for details); and (3) fMRI data did not pass quality control (see fMRI data preprocessing for details). Our behaviour criterion was based on the performance at the load 1 condition, which should be the easiest among the three task conditions. We used accuracy at the easiest condition to screen out participants who did not perform the task properly. Nine participants failed the behavioural performance requirement. Out of the remaining 61 participants, 48 participants had good quality fMRI data, among which 31 participants (mean age = 24.9, SD = 5.1, 16 females) had good EEG and fMRI data. We first determined the NSW component from these 31 participants.

### Spatial working memory task

We used the Sternberg delayed-match-to-sample task paradigm (Sternberg, 1966) consisting of three phases in each trial: encoding, retention, and probing. Unlike other paradigms such as the N-back task that led to overlapping of the encoding, retention and retrieval responses even in the EEG time domain, the Sternberg delayed-match-to-sample task paradigm allows a better separation of the retention phase in time without other distracting stimuli. Each trial began with a fixation cross in the center of the screen lasting for 500 ms. Depending on the load condition, 1, 3 or 5 white dots was/were presented sequentially on a 5-by-5 grid with 24 possible location of appearance (excluding central fixation), each lasting for 500 ms. A fixation cross was then displayed for 3000 ms (retention phase), which was followed by a red dot presented for 2000 ms (probing phase). Participants were required to indicate whether the red dot appeared at a previously occupied location. Between trials, a blank black screen was presented with a jittered inter-trial interval of 500–3500 ms. Each load consisted of 30 trials across 3 runs. Behavioural performance was indexed using Cowan's K (Cowan, 2001; Cowan et al., 2005), which is formulated as the difference between hit rate and false alarm rate, multiplied by the total number of presented items (i.e., load levels). In calculating K, it is assumed that if an individual can hold K items in memory given S items, task performance should be correct on K/S of the trials (i.e. if K is 4, and S is 5, it is expected that hit rate should be 80%). In the current formulation, false alarm rate is subtracted from the hit rate to account for guessing (Vogel et al., 2005). As K corresponds to a measure of capacity, the maximum K (K<sub>max</sub>) across the three load levels was used.

To investigate the association between EEG responses and individual differences in SWM capacity, we categorized participants into higher and

lower SWM capacity groups by applying median split on the Kmax (Vogel et al., 2005). Based on the sample of 31 participants who fulfilled the behaviour, EEG and fMRI criteria, the median of Kmax was 3.92 with 16 and 15 participants in the higher and the lower capacity groups respectively.

#### Data acquisition

Participants underwent a concurrent EEG-fMRI scanning session using 12-channel head coil on a 3T Siemens Tim Trio system (Siemens, Erlangen, Germany). The spatial working memory task fMRI scan consisted of 3 runs of echo planar imaging (EPI) volumes (TR/TE = 2000/30 ms, voxel size =  $3.0 \times 3.0 \times 3.0 \text{ mm}^3$ , FOV =  $192 \times 192 \text{ mm}^2$ , 36 axial slices, flip angle =  $90^\circ$ , 192 vol, bandwidth = 2112 Hz/pixel). High-resolution T1-weighted structure images (TR/TE/TI = 2300/2.98/900 ms, voxel size =  $1.0 \times 1.0 \times 1.0 \text{ mm}^3$ , FOV =  $256 \times 240 \text{ mm}^2$ , 192 continuous sagittal slices, flip angle =  $9^\circ$ , bandwidth = 240 Hz/pixel) were acquired using magnetization-prepared rapid gradient echo (MPRAGE) sequence for co-registration.

In parallel to fMRI recordings, concurrent EEG data were acquired using the 64-channel MRI-compatible EEG system (Brain Products GmpH, Germany) with proper synchronization and triggering. Positions of electrodes were based on the International 10–10 System (Jurcak et al., 2007) with online reference to FCz. The sampling frequency was at 5 KHz. One ECG electrode was placed at the fifth intercostal space on the midclavicular line at the back, while an EOG electrode was placed below left eye, vertically aligned to the F1 electrode. We also ensured that the impedance at all electrodes were below 10 KW. Helium-pump was switched off during concurrent EEG-fMRI recording to avoid related artefacts (Nierhaus et al., 2013).

#### EEG data preprocessing

Following previous work (Allen et al., 2000, 1998; Tong and Thakor, 2009), we removed both gradient artefacts and cardiobalistic artefacts using BrainVision Analyzer 2.0 (BrainProducts GmbH). For gradient artefacts, a representative template artefact was calculated and subtracted from a sliding window of 21 TRs (Allen et al., 2000). The EEG data were then down sampled to 250 Hz. For cardiobalistic artefacts, ECG episodes were first identified by the software using the amplitude and cross-correlation criteria peaks (Tong and Thakor, 2009). The identified R peaks were then visually verified/adjusted by trained researchers. Delay time between the ECG episodes and the cardiobalistic artefacts were calculated using global field power based on the entire dataset. Cardiobalistic artefact correction was done with a sliding window of 21 TRs (Allen et al., 1998). Further EEG data preprocessing was performed using in-house scripts based on EEGLab (version 13.4.3b) in Matlab (2010b). We used CleanLine to remove line noise. The low-pass filter at 90 Hz was applied followed by high-pass filtering at 0.1 Hz. Motion artefacts and noisy channels were rejected before performing Independent component analysis (ICA) to remove eye movement-related artefacts and the remaining of the cardiobalistic artefacts. Following channel interpolation, the data were re-referenced to the average of the scalp channels.

Epochs were identified with data time-locked to the onset of the retention period. Data in the 200 ms before retention onset served as the baseline, while the data time window was 3 s after retention onset. After baseline correction, epoch data were subjected to visual inspection to remove remaining noises. Only correct trials were included for further analyses. To identify the NSW ERP, we then re-reference the epoch data to the average of mastoids (TP9 and TP10).

EEG data from each participant were included for further analyses if all of the following requirements were met: (1) At least 70% of the epochs remained in the data after preprocessing; (2) Less than 33% of the channels were rejected during preprocessing; and (3) ERP was detected in the data ( $p \leq 0.05$ ) using the randomization-based procedure (Koenig et al., 2013).

#### Temporo-spatial principal component analysis

Retention EEG negativities can be a combination of NSW and other load-dependent ERP. These ERPs can be differentially affected by working memory loads and are related to different cognitive components (Fukuda et al., 2015; Zhou and Thomas, 2015). For example, NSW and P3 shared overlapping scalp distribution and temporal profiles, but are differentially affected by working memory load, with the former showing increasing component amplitude, and the latter showing decreasing component amplitude with increasing load (Zhang et al., 2015; Zhou and Thomas, 2015). Fortunately, recent studies of visual working memory demonstrated that temporal PCA could tease apart these temporally overlapping components and identify different components related to loads and SWM capacity (Dien, 2012; Pinal et al., 2014; Zhou and Thomas, 2015). Temporo-spatial PCA has been successful in identifying spatially and temporally overlapping components for other task paradigms such as the emotion regulation task (Liu et al., 2016) and the odd-ball task (Dien, 2012). Here, we used the temporo-spatial PCA methods to identify the NSW component related to both load and SWM capacity.

We applied temporo-spatial PCA (Dien, 2012; Kayser and Tenke, 2003; Liu et al., 2016) on ERPs from each participant and condition (see flowchart in Supplementary Fig. 1). Temporal PCA was first performed on the average ERP to reduce the data to the NSW-related time course. Here, time points were the variables, while channels, conditions and participants were the observations (i.e., one observation refers to data in one channel in one condition in a particular participant). Promax rotation method was used to separate variance orthogonally (Dien, 2010). Variance accounted by each temporal component was calculated and sorted. Only temporal components that explained more than 1% of the total variance were considered. We selected the temporal components that shared similar time courses with the NSW ERP. Spatial PCA was then performed separately on the factor scores (FS) obtained from each temporal component, which represented the variance of each channel, condition and participant in regard to the component.

For spatial PCA, channels were the variables, while conditions and participants were the observations. We performed spatial PCA in two steps. In step one, we first randomised the FS of the temporal component to generate a randomised dataset. We performed spatial PCA on the randomised data set equating the number of dimensions to the number of channels and calculated the variance explained by the resulted components. We repeated this randomization procedure 500 times, and calculated the average explained variance across randomization. We also performed a spatial PCA on the original FS data equating the number of dimensions to the number of channels and calculated the explained variance of each resulting component. We then used scree plot to identify the number of spatial components based on the original data that explained more variance than the randomization averages. In step two, spatial PCA was again performed on the original FS data, but with PCA dimensions reduced to the number found in the scree plot. Infomax was then used as the rotation method to separate variance (Dien, 2010). The resulting temporo-spatial components were sorted based on the explained variance, where component explaining the largest amount of variance was selected. For the selected component, we obtained an FS for each condition per participant for statistical analyses. We used the nlme R package to test the load effect on the FS and the multcomp R package for the repeated-measurement post hoc analyses.

#### EEG-capacity association

We first examined load-related changes in EEG response by calculating an FS slope for each participant by regressing his/her FS against SWM loads. Specifically, we fitted a linear line to the FS for each participant, and used the slope as an estimate of load-related FS changes. The larger the absolute values of the FS slope, the more the participant's EEG responses changed as SWM load increased.

To further examine the difference between the higher and lower SWM capacity groups, we performed a linear regression analysis on the Kmax against FS slopes with group assignment as the variable of interest. In particular, we are interested in the NSW during retention and its association with both task capacity and brain (de)-activations (see section 2.8). The NSW was expected to be sustained negative activity during retention, of which amplitudes increase with memory loads until reaching capacity. Our participants were from the healthy young adult population and their Kmax scores were all above 2. Thus, when more negative FS indicates larger NSW amplitude, we expected that NSW amplitude would show load-related effect (i.e., negative FS slope). Though the NSW component was identified based on the analyses across all participants, it was still possible that a minority of individuals did not elicit the typical load-related NSW. Therefore, to minimize such confounder, we excluded participants whose FS slopes were in opposite polarity (i.e., positive FS slope when more negative FS indicates larger NSW amplitude) and beyond 1.5 standard deviation from the group FS slope mean (2 higher capacity and 1 lower capacity participants). The remaining participants ( $N = 28$ ) were used for association analyses of NSW component with task capacity and fMRI activation/deactivation patterns. There were no differences in age ( $p = 0.911$ ) and gender (chi-square test  $X^2 = 1.286$ ,  $p = 0.257$ ) between the higher and lower capacity groups among these 28 participants.

#### fMRI data preprocessing

The SWM task fMRI data was preprocessed using the FMRIB Software library (FSL) (Jenkinson et al., 2012) and Analysis of Functional Neuroimages software programme (Cox, 1996), following the standard protocols in our previous work (Ng et al., 2016; Wang et al., 2016). Briefly, the steps are: (1) dropping the first 5 volumes where magnetic field has yet stabilized; (2) slice time correction to adjust interlaced scanning time difference, oblique, and orientation in space; (3) motion correction producing 6 motion parameters used later in the analyses; (4) skull stripping; (5) spatial smoothing at full-width half maximum (FWHM) of 6 mm; and (6) coregistration with the structural image using Boundary-Based Registration (BBR), and nonlinear (FNIRT) registration to the Montreal Neurological Institute (MNI) 152 standard space. For the structural data, we followed the following steps: (1) image noise reduction (SUSAN); (2) skull stripping using the Brain Extraction Tool (BET); (3) linear (FLIRT) and FNIRT registration to the MNI 152 standard space; and (4) segmentation of the brain into grey matter, white matter and CSF compartments.

Trained researcher visually inspected co-registration and normalization quality for all participants to ensure successful co-registration of the fMRI data to the T1-weighted structural images and to the MNI standard space. Importantly, one of the common sources of artefacts in the fMRI data is head motion during the scans. Therefore, for each volume in the fMRI data, we also calculated the absolute displacement from the reference volume and the relative displacement between volumes. We then identified the maximal absolute displacement and the maximal relative displacement for each participant as estimates of head motion. Since our original voxel size is 3 mm isotropic, we set the maximal absolute displacement cut-off at 3 mm and the maximal relative displacement cut-off at 1 mm to only include participants with limited head motion. After excluding participants whose data were beyond the cut-off, the average motion in our data sample is 0.57 mm ( $SD = 0.45$  mm) of maximal absolute displacement and 0.38 mm ( $SD = 0.25$  mm) of maximal relative displacement.

#### EEG-fMRI associations

Preprocessed functional data that passed quality control were analyzed using whole-brain voxel-wise general linear model (GLM) implemented in SPM8 (<http://www.fil.ion.ucl.ac.uk/spm/>). At the first level analysis, activations in the retention phases of each load were

modeled together with covariates of the six motion parameters. Correct and error trials were modeled separately. Event duration was set to be the same as the phase duration. Contrast images of the retention phase of the correct trials in each load condition was taken from each participant and carried forwards to the second level analysis. At the second level analysis, retention images were regressed against FS of the NSW component along with covariates of age and gender. Contrast images from the second level analyses were thresholded at the voxel-wise significance level of uncorrected  $p < 0.001$  and cluster-wise significance level of family-wise error (FWE) corrected  $p < 0.05$ . Association analyses were done within the higher and lower capacity groups. We also performed a GLM analysis on the deactivations using the same variables of interest and covariates at the first level and repeated the same second-level analyses on the deactivation contrasts.

## Results

### Load-related NSW PCA component

Preprocessed EEG data were averaged across trials but within channels, conditions and participants to obtain the NSW ERP. Fig. 1 showed the average NSW ERP components across all participants separated by memory load. Temporo-spatial PCA was conducted based on the ERP data. We obtained two temporal principal components (PCs) from the temporal PCA (Fig. 2), each of which explained more than 1% of variance. Among the obtained temporal components, we only considered those that explained more than 1% of the total variance. In total, six temporal components fulfilled this variance criteria. One component was restricted within the 200 ms baseline period. One component spiked at the onset of retention, while another component occupied the first 100 ms after retention onset, both of which were possibly related to offset of the dot from the encoding period. Another component spiked at the end of the retention period, possibly linked to probe onset. The remaining two temporal components (T1 and T2) spread across almost 2 s during retention period, with T2 occupying the first 2 s and T1 dominating the last 2 s of the retention period (Fig. 2). We labeled the component using letter and number. T indicates the component was obtained from the temporal PCA; number 1, 2, etc. indicate the component explained the largest, the second largest, etc. variance). Spatial PCA was then conducted on each of these two temporal PCs. The spatial components that explained the largest variance were selected.

As a result, we obtained two temporo-spatial PCs with anterior-posterior topographic scalp distribution (Fig. 2A). One peaked within the first second (T2S1) after retention onset, while the other loaded heavily towards the end of the retention phase (T1S1) (S indicates the component was obtained from the spatial PCA). T1S1 explained the largest variance of the temporal component T1, which was also the largest component from the temporal PCA. T2S1 explained the largest variance of the temporal component T2, which was the second largest component from the temporal PCA. Based on the time courses and the spatial distributions of the PCs, T1S1 is likely to be the NSW component.

Since the NSW ERP component is load-related, we further analyzed the FS from each temporo-spatial PCs with load as variable of interest. Only T1S1 showed significant main effect of load ( $F(2, 60) = 4.648$ ,  $p = 0.013$ ). Both load 3 ( $z = -2.682$ , adjusted  $p = 0.020$ ) and load 5 ( $z = -2.596$ , adjusted  $p = 0.023$ ) had greater negative FS than load 1. No significant difference between load 3 and load 5 was found ( $z = 0.086$ , adjusted  $p = 0.996$ ). There was no significant load effect on T2S1 ( $F(2, 60) = 2.413$ ,  $p = 0.098$ ). This confirmed that the NSW component identified (T1S1) is related to memory load.

### Load-related NSW increase was differentially associated with SWM capacity in higher and lower capacity groups

To test whether the load effect on the NSW component amplitudes differed between capacity groups, we analyzed the effect of memory

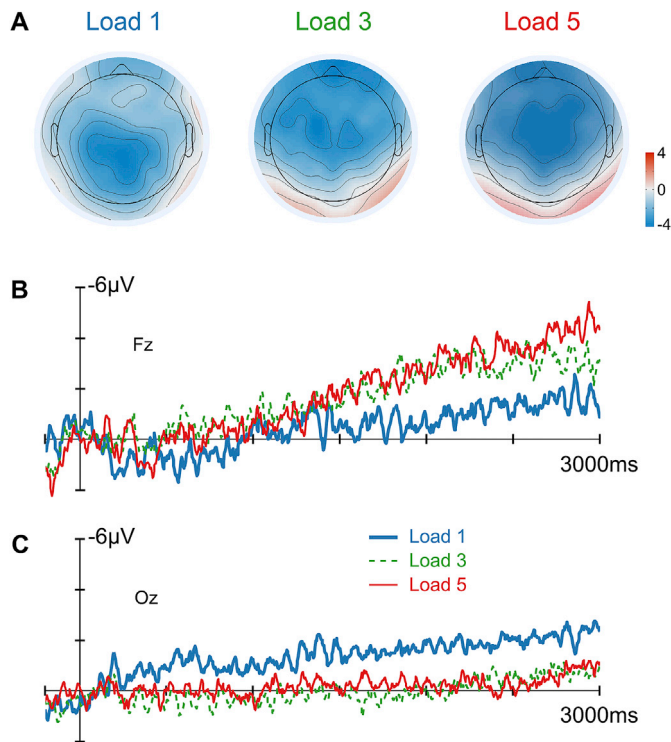


**Fig. 1.** ERP responses during retention. (A) Topographic scalp distribution of the ERP responses during retention. Blue colour indicates negative amplitudes and red colour indicates positive amplitudes in  $\mu$ Volt. ERP amplitudes between 2000 ms and 3000 ms after retention onset were averaged for each SWM load. As loads increased, negativity became more salient over the fronto-parietal scalp area. (B) ERP responses at the Fz channel. ERP responses averaged across all participants within each load at the Fz channel time locked to the onset of retention period. Sustained negative activities developed during retention and showed higher amplitudes towards the end of retention. (C) ERP responses at the Oz channel. ERP responses averaged across all participants within each load at the Oz channel time locked to the onset of retention. For Fig. 1B and C, thick solid blue lines show the ERP at load 1; thin dotted green lines show the ERP at load 3; and thin solid red lines show the ERP at load 5. Abbreviations: ERP = event-related potential, NSW = negative slow wave, SWM = spatial working memory.

loads and capacity groups on FS using this sample of 28 participants. The interaction between capacity groups and loads was not significant ( $F(2, 52) = 0.099, p = 0.906$ ), and neither was the main effect of groups significant ( $F(1, 26) = 0.102, p = 0.752$ ). The main effect of loads was significant ( $F(2, 52) = 14.391, p < 0.001$ ). Both load 3 ( $z = -4.545, \text{adjusted } p < 0.001$ ) and load 5 ( $z = -4.888, \text{adjusted } p < 0.001$ ) had greater negative FS than load 1. No significant difference between load 3 and load 5 was found ( $z = -0.343, \text{adjusted } p = 0.937$ ).

More importantly, we found significant FS slope-by-group interaction effect on  $K_{\text{max}}$  ( $p = 0.005$ ), as well as significant main effect of FS slopes ( $p = 0.010$ ) and participant groups ( $p = 0.012$ ) on  $K_{\text{max}}$ . Steeper FS slopes were correlated with higher  $K_{\text{max}}$  in higher capacity group (adjusted  $R^2 = 0.325, p = 0.020$ , Fig. 3B), while steeper FS slopes were correlated with lower  $K_{\text{max}}$  in the lower capacity group (adjusted  $R^2 = 0.257, p = 0.037$ , Fig. 3A).

We repeated the analyses using the new cut-off (median of  $K_{\text{max}} = 3.67$  based on all participants ( $N = 61$ ) who fulfilled the task accuracy criteria regardless of their imaging data quality). Our main findings remained unchanged (see Supplementary Results 2). Consistent with the interaction effect, we also found a significant quadratic relationship between  $K_{\text{max}}$  and FS slopes across all participants (Supplementary Fig. 2).

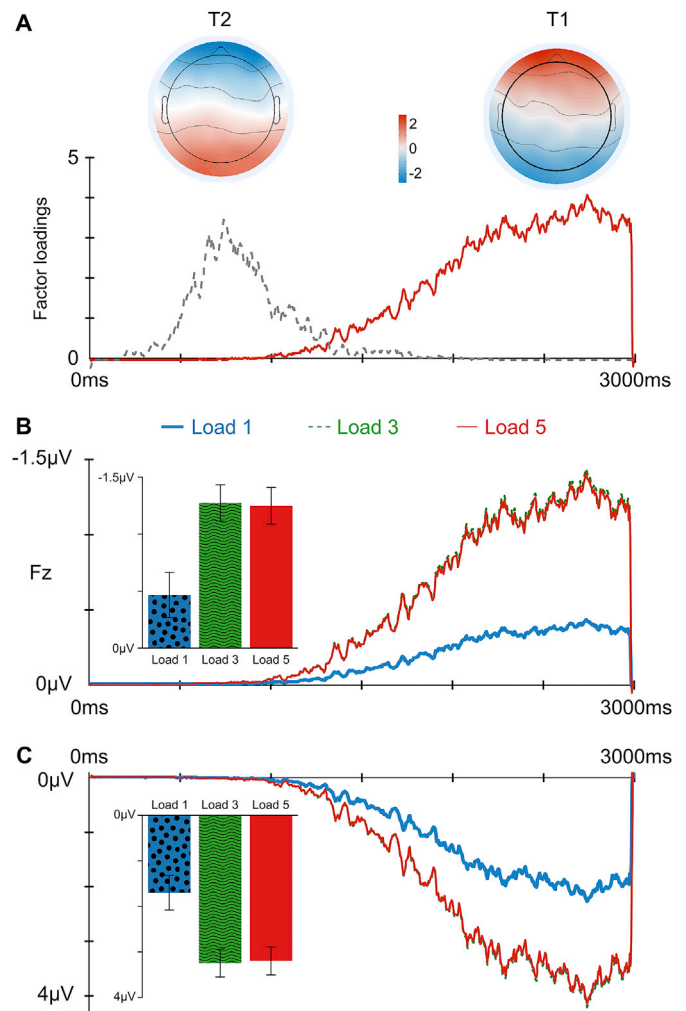


**Fig. 2.** Amplitudes of the NSW component from temporo-spatial PCA were different between SWM loads. (A) Temporal loadings and scalp distribution of the PCA components. Only the NSW component (T1) was related to SWM loads. (B) NSW component projection to the Fz channel. (C) NSW component projection to the Oz channel. FS at load 3 and 5 were significantly different from FS at load 1. For both Fig. 2B and C, thick solid blue lines shows the component projection at load 1; thin dotted green lines shows the component projection at load 3; and thin solid red lines shows the component projection at load 5. Abbreviations: NSW = negative slow wave, PCA = principal component analysis, SWM = spatial working memory, FS = factor score, T1 = the temporal component that explained the largest variance, T2 = the temporal component that explained the second largest variance.

#### Different NSW-related brain networks were recruited by higher and lower capacity participants

To examine the difference in brain networks recruited by the higher and lower capacity participants, we compared whole-brain voxel-wise activation and deactivation across SWM loads in each capacity group. Higher activation in the FPN and more deactivation in DMN for higher SWM loads were observed for the higher capacity participants (Supplementary Table 1). Though load-related FPN activation differences were also found for the lower capacity participants, deactivation in DMN were not significantly related to load (Supplementary Table 2).

Importantly, we further examined the brain networks contributing to the NSW component related to SWM loads, by looking at the associations of the NSW component with the fMRI-based activation and deactivation patterns in higher and lower capacity groups. For the high capacity participants, whole-brain voxel-wise GLM regression against NSW FS

revealed that greater negative FS (i.e., larger NSW component amplitude) was associated with higher activations in the bilateral parietal areas (FPN) (Fig. 4A and B) and deactivation in the medial prefrontal and mid-cingulate areas (DMN) (Fig. 4C and D, Supplementary Table 3). In contrast, for lower capacity group, no such association was found. Instead, greater negative FS was related to higher deactivation in the right middle temporal gyrus (Fig. 5, Supplementary Table 4). We repeated the analyses using the new cut-off (median of  $K_{max} = 3.67$  based on all participants ( $N = 61$ ) who fulfilled the task accuracy criteria regardless of their imaging data quality). Our main findings remained unchanged (see Supplementary Results 2, Supplementary Tables 6 and 7, Supplementary Figs. 3 and 4).

## Discussion

Between the phase of information encoding and the time to retrieve the information lies the important phase of retention, where information that is no longer present in the external environment must be carried in mind. We recorded concurrent EEG-fMRI responses when participants performed a spatial working memory task to examine retention-related sustained negative response and the associated brain networks underlying individual differences in SWM capacity. Specifically, using temporospatial PCA method, we isolated the NSW principle component during retention that elicited larger amplitudes for higher SWM loads. Load-related NSW changes were associated with both SWM capacity and brain activation/deactivations differently in higher and lower capacity participants. For higher SWM capacity participants, stronger activation in the FPN and more deactivation in the DMN correlated with larger NSW amplitudes. Larger NSW increase with loads supported better task capacity. In contrast, for lower SWM capacity participants, NSW amplitudes were linked to neither FPN nor DMN. Instead, NSW amplitudes changed with right MTG deactivation. Larger load-related changes in NSW were linked with worse task capacity. Our results suggested that distinct brain networks underlie individual differences in human spatial working memory capacity.

### Neural substrates underlying SWM individual differences

For higher capacity participants, the increase in NSW PC amplitude, from low to high loads, was associated with larger activation/deactivation in the brain areas of the SWM-related networks (i.e., FPN and DMN). The FPN is considered a task-positive network (Ptak, 2012), which has been associated with working memory. Activation in bilateral parietal regions from the FPN was larger in load 3 and load 5 compared to in load 1. On the other hand, the DMN is considered a task-negative network (Raichle et al., 2001; Uddin et al., 2009). Brain regions in the DMN are

often deactivated during task performance including retention in working memory task (Piccoli et al., 2015). Consistent with the existing literature, we found that higher NSW PC amplitudes were correlated with greater activation in bilateral parietal regions (the FPN regions) and deactivation in middle cingulate cortex, supplementary motor area, and medial frontal gyrus (the DMN regions) among higher capacity participants.

Furthermore, load-related amplitude increase of the NSW PC was also related to better SWM capacity, supporting previous findings that NSW can reflect individual difference in working memory capacity (Vogel and Machizawa, 2004). Interestingly, our results are also consistent with findings in younger populations, where younger participants (age 9–12) were tested with N-back task (Huang et al., 2016). It was found that better SWM capacity was associated with higher load-related deactivation in the DMN network (including PCC/MCC and medial prefrontal cortex) and tentatively with higher load-related activation in the FPN network (e.g., inferior parietal lobe). The load-related deactivation was also correlated with their executive functions measured at the earlier ages (age 3–9). Along a similar note, our study showed that young adults with higher SWM capacity elicited larger NSW PC responses in higher than lower SWM load, which were related to higher activation in the FPN regions and larger deactivation in the DMN regions. Taken together, our findings suggested that better segregation between task-positive and the task-negative brain networks could support greater SWM capacities.

In contrast to individuals with higher capacity, the NSW PC did not exhibit the same association with the brain activation/deactivation for lower capacity participants. While the lower capacity group also showed higher activation in the FPN with higher SWM load, activity in the FPN was not associated with the NSW PC. Additionally, the lower capacity group also did not exhibit load-related deactivation in the DMN. Interestingly, a recent study also reported decrease of DMN suppression among the elderly, when performing tasks that showed age-related performance decline, but not for the tasks where performance did not change with age (Samu et al., 2017). In our study, a different region (i.e., right posterior MTG) was correlated with the NSW PC, and more deactivation in the right posterior MTG was linked to more negative FS (larger NSW PC amplitudes). Right MTG has been linked to both the DMN and the semantic/language network. Recent study using tractography-based parcellation methods suggested that posterior MTG was more likely to be part of the language network (Davey et al., 2016). Our results suggested that lower capacity participants might recruit different brain networks in the SWM task, which might be indicative of less optimal strategy. Larger NSW PC amplitude changes with increasing load were correlated with their poorer SWM capacity. These suggest that the involvement of different neural substrates may underlie the poorer capacity in the lower capacity group.

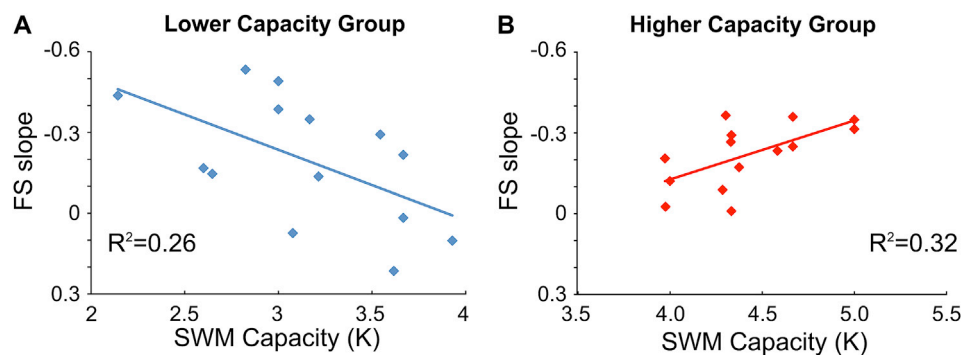


**Fig. 3.** Association between NSW component and SWM capacity. A) Lower SWM capacity group: Larger NSW FS slopes were related lower SWM capacity. B) Higher SWM capacity group: Larger NSW FS slopes were related to higher SWM capacity. Abbreviations: NSW = negative slow wave, SWM = spatial working memory, FS = factor score,  $K_{max}$  = maximum Cowen's K.

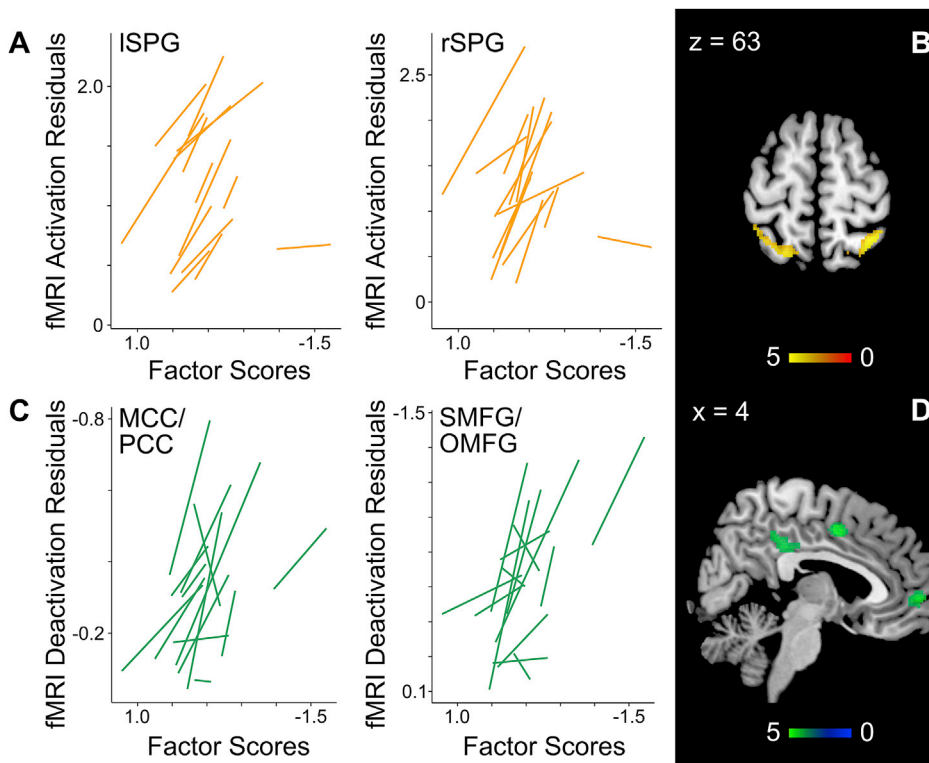


**Fig. 4.** Association between NSW component and BOLD responses in higher SWM capacity group. Larger NSW component amplitudes were related to higher activations in bilateral parietal regions (ISPG and rSPG) within FPN (A and B) and larger deactivation in PCC/MCC and SMFG/OMFG within DMN (C and D). In Fig. 4A, more negative FS at the X axis indicates larger NSW amplitude. Y axis shows activation in the FPN regions after controlling for age and gender, where more positive value indicates higher activation. In Fig. 4C, more negative FS at the X axis indicates larger NSW amplitude. Y axis shows the deactivation in the DMN regions after controlling for age and gender, where more negative value indicates larger deactivation. In both 4A and 4C, each line represents one participant, where a linear line was fitted to the activation or the deactivation against FS for each participant. Fig. 4B shows the bilateral parietal regions where FS were significantly correlated with the brain activation. Fig. 4D shows the DMN regions where FS were significantly correlated with the brain deactivation. In both 4B and 4D, the colour bars indicate the z values from the correlation contrasts. Abbreviations: NSW = negative slow wave, BOLD = blood-oxygen-level dependent, SWM = spatial working memory, ISPG = left superior parietal gyrus, rSPG = right superior parietal gyrus, FPN = fronto-parietal network, PCC = posterior cingulate cortex, MCC = middle cingulate cortex, SMFG = superior medial frontal gyrus, OMFG = orbital medial frontal gyrus, DMN = default mode network.

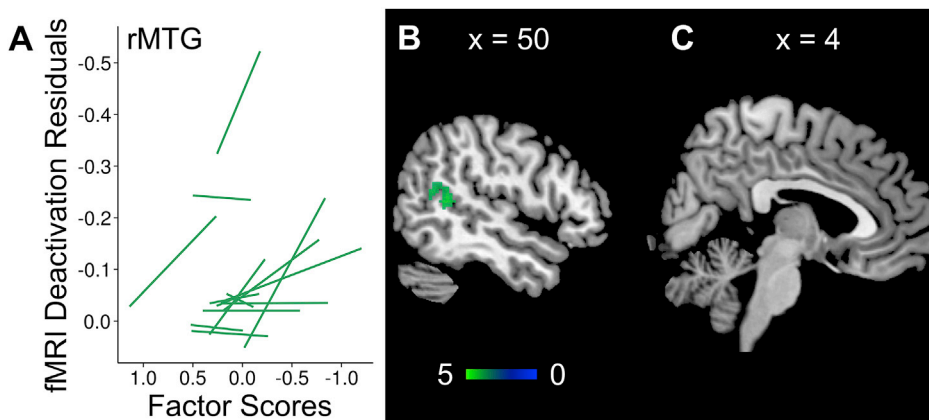


**Fig. 5.** Association between NSW component and BOLD responses in lower SWM capacity group. Larger NSW component amplitudes were related to larger deactivation in the rMTG. In Fig. 5A, more negative FS at the X axis indicates larger NSW amplitude. Y axis shows the deactivation in the DMN regions after controlling for age and gender, where more negative value indicates larger deactivation. Each line represents one participant, where a linear line was fitted to the deactivation against FS for each participant. Fig. 5B shows the rMTG region where FS were significantly correlated with the brain deactivation. Fig. 5C shows that the DMN regions where FS were significantly correlated with the brain deactivation in the higher capacity group were not significant in the lower capacity group. Results were reported at the threshold level of voxel-wise uncorrected  $p < 0.001$  and cluster-wise FWE corrected  $p < 0.05$ . The colour bar indicates the z values from the correlation contrasts. Abbreviations: NSW = negative slow wave, BOLD = blood-oxygen-level dependent, SWM = spatial working memory, rMTG = right middle temporal gyrus, DMN = default mode network, FS = factor score, FWE = family-wise error.

#### Selective attention and disruption suppression of working memory

Current analyses focused on the retention period in working memory task, when stimuli were no longer present in the external environment. To successfully retain the memory representations in the brain, selective attention and distractor inhibition are important besides sufficient storage capacity. Higher memory load exhausting attentional resources could

possibly limit participants' SWM capacity. Failure to inhibit distraction at higher memory load could be linked to reduced signal-to-noise ratio of the brain networks (Durstewitz and Seamans, 2008), which could also be harmful to the task performance.

While previous fMRI studies have pointed to related brain networks, EEG studies on responses in the frequency domain also identified the associated changes in power, phase and peak frequencies. For example,

gamma responses, which have been suggested to be originating from the frontal and parietal cortices based on source localization (Roux et al., 2012), were linked to working memory load changes, reflecting the active maintenance of the visual spatial information (Roux and Uhlhaas, 2014). On the other hand, fronto-medial theta power with source localization pointing to the medial frontal and ACC regions (Palva et al., 2011) were predictive of task accuracy (Maurer et al., 2015). Alpha power and peak frequency were likely to play a role in inhibiting disruption, especially at the later stage of retention (Maurer et al., 2015; Xie et al., 2016). Granger causality analysis suggested that alpha-range activities flow from frontal to parietal regions during retention of spatial information (Protopapa et al., 2014). Enhancing alpha activities over the task-irrelevant parietal area using TMS-EEG methods improved working memory performance (Sauseng et al., 2009). These results from the frequency domain suggested that both fast and slow neural responses contributed to SWM processes but with different functions of selective attention and disruption inhibition. Complementarily, our study, focusing on the time domain of the neural responses, identified both early and late responses during retention period. However, only the late response developing throughout the retention period co-varied with load increase. This late response was correlated with activation and deactivation of brain networks related to selective attention and distractor suppression in higher capacity participants.

We used the Sternberg task, which has been used in many working memory studies since it was developed in 1966 (Sternberg, 1966). It has several advantages over other common task paradigms such as the lateral cueing paradigm and the N-back task. First, Sternberg task has no task-irrelevant stimuli presented together with items to be remembered. Load related changes in both behavioural and brain responses were less likely due to task-irrelevant competing stimuli in the external environment. Interestingly, we found significant load effect on the DMN deactivations in the higher SWM capacity group but not in the lower capacity group. Second, longer retention duration in the task allowed the NSW to develop while differentiating it from the other earlier ERP components. Early and late portions of the retention duration may be linked to different processes in SWM. Consistent with findings from the frequency domain, the load-related increase of the late neural responses corresponded to the patterns of the concurrently recorded activation and deactivation changes in the FPN and DMN among higher capacity participants. While FPN was related to selective attention, DMN was linked to distractor suppression (Chadick and Gazzaley, 2011; Zanto and Gazzaley, 2009). This suggests that the late NSW responses may be related to the synchronization across the different brain networks supporting diverse functions that promote better spatial working memory capacity.

#### Future directions and conclusion

There remain several opportunities for future research. First, we divided our participants into higher and lower capacity groups based on a median split of the SWM capacity. The median was 3.92 indicating a capacity of about 4 spatial locations. Four active representations were also suggested as the average capacity limit of human working memory by Cowan (Cowan, 2010, 2001). Thus, our capacity groups could represent samples of young adults that had SWM capacity either higher or lower than the average of the general young adult population. Integration of fMRI and EEG promises to provide better temporal and spatial information of the neural substrates underlying individual differences in spatial working memory among various populations. Longitudinal study with larger sample could follow to further understand the related developmental or pathological changes of the brain.

Second, the current task tends to activate processes related to maintenance of the memory representations rather than manipulations or updating (Bray et al., 2015; Gorgoraptis et al., 2011; Veltman et al., 2003). Future research could examine the individual differences in the temporal and spatial profiles of the SWM processes for manipulation and

updating. In the current study, performance on each trial was quantified in a binarised manner, but it is possible that more precise measures (e.g., degree of error) can be used in future studies, in conjunction with probabilistic models, to better quantify such individual differences (Gorgoraptis et al., 2011; Ma et al., 2014).

Third, our EEG-fMRI analyses focused on correct trials only. Nevertheless, different sources of errors may give insight on the processes that limited the SWM capacity. Experiment designs that induce more error trials can be used to examine the sources of errors that limit the SWM capacity.

In conclusion, we identified the NSW component during SWM retention using PCA and demonstrated that it was linked to individual differences in SWM capacity and both functional activation and deactivation patterns. Our findings suggest that participants with high and low SWM capacity may utilize differential NSW-related neural networks for memory maintenance.

#### Acknowledgements

We would like to thank all participants for their participation in this study. This work was supported by the National Medical Research Council, Singapore (NMRC/CBRG/0088/2015 to JZ), and Duke-NUS Medical School Signature Research Program funded by Ministry of Health, Singapore.

#### Appendix A. Supplementary data

Supplementary data related to this article can be found at <https://doi.org/10.1016/j.neuroimage.2018.04.014>.

#### References

- Alavash, M., Doebler, P., Holling, H., Thiel, C.M., Gießing, C., 2015. Is functional integration of resting state brain networks an unspecific biomarker for working memory performance? *NeuroImage* 108, 182–193. <https://doi.org/10.1016/j.neuroimage.2014.12.046>.
- Allen, P.J., Josephs, O., Turner, R., 2000. A method for removing imaging artifact from continuous EEG recorded during functional MRI. *NeuroImage* 12, 230–239. <https://doi.org/10.1006/nimg.2000.0599>.
- Allen, P.J., Polizzi, G., Krakow, K., Fish, D.R., Lemieux, L., 1998. Identification of EEG events in the MR scanner: the problem of pulse artifact and a method for its subtraction. *NeuroImage* 8, 229–239. <https://doi.org/10.1006/nimg.1998.0361>.
- Anguera, J.A., Reuter-Lorenz, P.A., Willingham, D.T., Seidler, R.D., 2010. Failure to engage spatial working memory contributes to age-related declines in visuospatial learning. *J. Cogn. Neurosci.* 23, 11–25. <https://doi.org/10.1162/jocn.2010.21451>.
- Ashkenazi, S., Rosenberg-Lee, M., Metcalfe, A.W.S., Swigart, A.G., Menon, V., 2013. Visuo-spatial working memory is an important source of domain-general vulnerability in the development of arithmetic cognition. *Neuropsychologia* 51, 2305–2317. <https://doi.org/10.1016/j.neuropsychologia.2013.06.031>.
- Bray, S., Almas, R., Arnold, A.E.G.F., Iaria, G., MacQueen, G., 2015. Intraparietal sulcus activity and functional connectivity supporting spatial working memory manipulation. *Cereb. Cortex* 25, 1252–1264. <https://doi.org/10.1093/cercor/bht320>.
- Burzynska, A.Z., Nagel, I.E., Preuschhof, C., Li, S.-C., Lindenberger, U., Bäckman, L., Heekeren, H.R., 2011. Microstructure of frontoparietal connections predicts cortical responsivity and working memory performance. *Cereb. Cortex* 21, 2261–2271. <https://doi.org/10.1093/cercor/bhq293>.
- Chadick, J.Z., Gazzaley, A., 2011. Differential coupling of visual cortex with default network or frontal-parietal network based on goals. *Nat. Neurosci.* 14, 830–832. <https://doi.org/10.1038/nn.2823>.
- Constantinidis, C., Klingberg, T., 2016. The neuroscience of working memory capacity and training. *Nat. Rev. Neurosci.* 17, 438–449. <https://doi.org/10.1038/nrn.2016.43>.
- Cowan, N., 2010. The magical mystery four: how is working memory capacity limited, and why? *Curr. Dir. Psychol. Sci.* 19, 51–57. <https://doi.org/10.1177/0963721409359277>.
- Cowan, N., 2001. The magical number 4 in short-term memory: a reconsideration of mental storage capacity. *Behav. Brain Sci.* 24, 87–114. <https://doi.org/10.1017/S0140525X01003922>.
- Cowan, N., Elliott, E.M., Saults, J.S., Morey, C.C., Mattox, S., Hismjatullina, A., Conway, A.R.A., 2005. On the capacity of attention: its estimation and its role in working memory and cognitive aptitudes. *Cogn. Psychol.* 51, 42–100. <https://doi.org/10.1016/j.cogpsych.2004.12.001>.
- Cox, R.W., 1996. AFNI: software for analysis and visualization of functional magnetic resonance neuroimages. *Comput. Biomed. Res. Int. J.* 29, 162–173.

- Darkey, F., Klingberg, T., 2015. The role of fronto-parietal and fronto-striatal networks in the development of working memory: a longitudinal study. *Cereb. Cortex* 25, 1587–1595. <https://doi.org/10.1093/cercor/bht352>.
- Davey, J., Thompson, H.E., Hallam, G., Karapanagiotidis, T., Murphy, C., De Caso, I., Krieger-Redwood, K., Bernhardt, B.C., Smallwood, J., Jefferies, E., 2016. Exploring the role of the posterior middle temporal gyrus in semantic cognition: integration of anterior temporal lobe with executive processes. *Neuroimage* 137, 165–177. <https://doi.org/10.1016/j.neuroimage.2016.05.051>.
- Dien, J., 2012. Applying principal components analysis to event-related potentials: a tutorial. *Dev. Neuropsychol.* 37, 497–517. <https://doi.org/10.1080/87565641.2012.697503>.
- Dien, J., 2010. Evaluating two-step PCA of ERP data with geomin, infomax, oblimin, promax, and varimax rotations. *Psychophysiology* 47, 170–183. <https://doi.org/10.1111/j.1469-8986.2009.00885.x>.
- Drew, T.W., McCollough, A.W., Vogel, E.K., 2006. Event-related potential measures of visual working memory. *Clin. EEG Neurosci.* 37, 286–291. <https://doi.org/10.1177/155005940603700405>.
- Durstewitz, D., Seamans, J.K., 2008. The dual-state theory of prefrontal cortex dopamine function with relevance to catechol-O-methyltransferase genotypes and schizophrenia. *Biol. Psychiatry* 64, 739–749. <https://doi.org/10.1016/j.biopsych.2008.05.015>.
- Ekman, M., Fiebach, C.J., Melzer, C., Tittgemeyer, M., Derrfuss, J., 2016. Different roles of direct and indirect frontoparietal pathways for individual working memory capacity. *J. Neurosci.* 36, 2894–2903. <https://doi.org/10.1523/JNEUROSCI.1376-14.2016>.
- Ester, E.F., Sprague, T.C., Serences, J.T., 2015. Parietal and frontal cortex encode stimulus-specific mnemonic representations during visual working memory. *Neuron* 87, 893–905. <https://doi.org/10.1016/j.neuron.2015.07.013>.
- Fukuda, K., Mance, I., Vogel, E.K., 2015.  $\alpha$  power modulation and event-related slow wave provide dissociable correlates of visual working memory. *J. Neurosci.* 35, 14009–14016. <https://doi.org/10.1523/JNEUROSCI.5003-14.2015>.
- Fusar-Poli, P., Broome, M.R., Matthiasson, P., Woolley, J.B., Johns, L.C., Tabraham, P., Bramon, E., Valmaggia, L., Williams, S.C., McGuire, P., 2010. Spatial working memory in individuals at high risk for psychosis: longitudinal fMRI study. *Schizophr. Res.* 123, 45–52. <https://doi.org/10.1016/j.schres.2010.06.008>.
- Galashan, D., Fehr, T., Herrmann, M., 2015. Differences between target and non-target probe processing — combined evidence from fMRI, EEG and fMRI-constrained source analysis. *NeuroImage* 111, 289–299. <https://doi.org/10.1016/j.neuroimage.2015.02.044>.
- Gazzaley, A., Nobre, A.C., 2012. Top-down modulation: bridging selective attention and working memory. *Trends Cogn. Sci.* 16, 129–135. <https://doi.org/10.1016/j.tics.2011.11.014>.
- Gordon, E.M., Stollstorff, M., Vaidya, C.J., 2012. Using spatial multiple regression to identify intrinsic connectivity networks involved in working memory performance. *Hum. Brain Mapp.* 33, 1536–1552. <https://doi.org/10.1002/hbm.21306>.
- Gorgoraptis, N., Catalao, R.F.G., Bays, P.M., Husain, M., 2011. Dynamic updating of working memory resources for visual objects. *J. Neurosci.* 31, 8502–8511. <https://doi.org/10.1523/JNEUROSCI.0208-11.2011>.
- Hoffmann, S., Labrenz, F., Themann, M., Wascher, E., Beste, C., 2014. Crosslinking EEG time-frequency decomposition and fMRI in error monitoring. *Brain Struct. Funct.* 219, 595–605. <https://doi.org/10.1007/s00429-013-0521-y>.
- Huang, A.S., Klein, D.N., Leung, H.-C., 2016. Load-related brain activation predicts spatial working memory performance in youth aged 9–12 and is associated with executive function at earlier ages. *Dev. Cogn. Neurosci.* 17, 1–9. Special Section: The Developmental Neuroscience of Adolescence: Revisiting, Refining, and Extending Seminal Models. <https://doi.org/10.1016/j.dcn.2015.10.007>.
- Jenkinson, M., Beckmann, C.F., Behrens, T.E.J., Woolrich, M.W., Smith, S.M., 2012. FSL. *Neuroimage* 62, 782–790, 20 years of fMRI. <https://doi.org/10.1016/j.neuroimage.2011.09.015>.
- Jorge, J., van der Zwaag, W., Figueiredo, P., 2014. EEG–fMRI integration for the study of human brain function. *Neuroimage* 102 (Part 1), 24–34. <https://doi.org/10.1016/j.neuroimage.2013.05.114>.
- Jurcak, V., Tsuzuki, D., Dan, I., 2007. 10/20, 10/10, and 10/5 systems revisited: their validity as relative head-surface-based positioning systems. *Neuroimage* 34, 1600–1611. <https://doi.org/10.1016/j.neuroimage.2006.09.024>.
- Kane, M.J., Engle, R.W., 2002. The role of prefrontal cortex in working-memory capacity, executive attention, and general fluid intelligence: an individual-differences perspective. *Psychon. Bull. Rev.* 9, 637–671. <https://doi.org/10.3758/BF03196323>.
- Kayser, J., Tenke, C.E., 2003. Optimizing PCA methodology for ERP component identification and measurement: theoretical rationale and empirical evaluation. *Clin. Neurophysiol.* 114, 2307–2325. [https://doi.org/10.1016/S1388-2457\(03\)00241-4](https://doi.org/10.1016/S1388-2457(03)00241-4).
- Koenig, T., Stein, M., Grieder, M., Kottlow, M., 2013. A tutorial on data-driven methods for statistically assessing ERP topographies. *Brain Topogr.* 27, 72–83. <https://doi.org/10.1007/s10548-013-0310-1>.
- Ku, Y., Bodner, M., Zhou, Y.-D., 2015. Prefrontal cortex and sensory cortices during working memory: quantity and quality. *Neurosci. Bull.* 31, 175–182. <https://doi.org/10.1007/s12264-014-1503-7>.
- Lenartowicz, A., Delorme, A., Walshaw, P.D., Cho, A.L., Bilder, R.M., McGough, J.J., McCracken, J.T., Makeig, S., Loo, S.K., 2014. Electroencephalography correlates of spatial working memory deficits in attention-deficit/hyperactivity disorder: vigilance, encoding, and maintenance. *J. Neurosci.* 34, 1171–1182. <https://doi.org/10.1523/JNEUROSCI.1765-13.2014>.
- Linden, D.E.J., Bittner, R.A., Muckli, L., Waltz, J.A., Kriegeskorte, N., Goebel, R., Singer, W., Munk, M.H.J., 2003. Cortical capacity constraints for visual working memory: dissociation of fMRI load effects in a fronto-parietal network. *NeuroImage* 20, 1518–1530. <https://doi.org/10.1016/j.neuroimage.2003.07.021>.
- Liu, S., Vanderhassel, M.-A., Zhou, J., Schirmer, A., 2016. Better not to know? Emotion regulation fails to benefit from affective cueing. *Front. Hum. Neurosci.* 10, 599. <https://doi.org/10.3389/fnhum.2016.00599>.
- Luck, S.J., Vogel, E.K., 2013. Visual working memory capacity: from psychophysics and neurobiology to individual differences. *Trends Cogn. Sci.* 17, 391–400. <https://doi.org/10.1016/j.tics.2013.06.006>.
- Ma, W.J., Husain, M., Bays, P.M., 2014. Changing concepts of working memory. *Nat. Neurosci.* 17, 347–356. <https://doi.org/10.1038/nn.3655>.
- Marchand, Y., Lefebvre, C.D., Connolly, J.F., 2006. Correlating digit span performance and event-related potentials to assess working memory. *Int. J. Psychophysiol.* 62, 280–289. <https://doi.org/10.1016/j.ijpsycho.2006.05.007>.
- Maurer, U., Brem, S., Liechi, M., Maurizio, S., Michels, L., Brandeis, D., 2015. Frontal midline theta reflects individual task performance in a working memory task. *Brain Topogr.* 28, 127–134. <https://doi.org/10.1007/s10548-014-0361-y>.
- Michels, L., Luchinger, R., Koenig, T., Martin, E., Brandeis, D., 2012. Developmental changes of BOLD signal correlations with global human EEG power and synchronization during working memory. *PLoS One* 7. <https://doi.org/10.1371/journal.pone.0039447>.
- Miller, B.T., Deouell, L.Y., Dam, C., Knight, R.T., D'Esposito, M., 2008. Spatio-temporal dynamics of neural mechanisms underlying component operations in working memory. *Brain Res.* 1206, 61–75. <https://doi.org/10.1016/j.brainres.2008.01.059>.
- Mizuhara, H., Sato, N., Yamaguchi, Y., 2015. Cortical networks dynamically emerge with the interplay of slow and fast oscillations for memory of a natural scene. *NeuroImage* 111, 76–84. <https://doi.org/10.1016/j.neuroimage.2015.02.019>.
- Nagel, I.E., Preuschhof, C., Li, S.-C., Nyberg, L., Bäckman, L., Lindenberger, U., Heekeren, H.R., 2009. Performance level modulates adult age differences in brain activation during spatial working memory. *Proc. Natl. Acad. Sci.* 106, 22552–22557. <https://doi.org/10.1073/pnas.0908238106>.
- Ng, K.K., Lo, J.C., Lim, J.K.W., Chee, M.W.L., Zhou, J., 2016. Reduced functional segregation between the default mode network and the executive control network in healthy older adults: a longitudinal study. *NeuroImage* 133, 321–330. <https://doi.org/10.1016/j.neuroimage.2016.03.029>.
- Nierhaus, T., Gundlach, C., Goltz, D., Thiel, S.D., Pleger, B., Villringer, A., 2013. Internal ventilation system of MR scanners induces specific EEG artifact during simultaneous EEG–fMRI. *NeuroImage* 74, 70–76. <https://doi.org/10.1016/j.neuroimage.2013.02.016>.
- Palva, J.M., Monto, S., Kulashakar, S., Palva, S., 2010. Neuronal synchrony reveals working memory networks and predicts individual memory capacity. *Proc. Natl. Acad. Sci.* 107, 7580–7585. <https://doi.org/10.1073/pnas.0913113107>.
- Palva, S., Kulashakar, S., Hämäläinen, M., Palva, J.M., 2011. Localization of cortical phase and amplitude dynamics during visual working memory encoding and retention. *J. Neurosci.* 31, 5013–5025. <https://doi.org/10.1523/JNEUROSCI.5592-10.2011>.
- Park, S., Holzman, P.S., 1992. Schizophrenics show spatial working memory deficits. *Arch. Gen. Psychiatry* 49, 975–982. <https://doi.org/10.1001/archpsyc.1992.01820120063009>.
- Piccoli, T., Valente, G., Linden, D.E.J., Re, M., Esposito, F., Sack, A.T., Salle, F.D., 2015. The default mode network and the working memory network are not anti-correlated during all phases of a working memory task. *PLoS One* 10. <https://doi.org/10.1371/journal.pone.0123354>.
- Pinal, D., Zurrón, M., Díaz, F., 2014. Effects of load and maintenance duration on the time course of information encoding and retrieval in working memory: from perceptual analysis to post-categorization processes. *Front. Hum. Neurosci.* 8, 165. <https://doi.org/10.3389/fnhum.2014.00165>.
- Protopapa, F., Siettos, C.I., Evdokimidis, I., Smyrnis, N., 2014. Granger causality analysis reveals distinct spatio-temporal connectivity patterns in motor and perceptual visuo-spatial working memory. *Front. Comput. Neurosci.* 8, 146. <https://doi.org/10.3389/fncom.2014.00146>.
- Ptak, R., 2012. The frontoparietal attention network of the human brain action, saliency, and a priority map of the environment. *Neurosci.* 18, 502–515. <https://doi.org/10.1177/1073858411409051>.
- Raichle, M.E., MacLeod, A.M., Snyder, A.Z., Powers, W.J., Gusnard, D.A., Shulman, G.L., 2001. A default mode of brain function. *Proc. Natl. Acad. Sci.* 98, 676–682. <https://doi.org/10.1073/pnas.98.2.676>.
- Rawdon, C., Murphy, J., Blanchard, M.M., Kelleher, I., Clarke, M.C., Kavanagh, F., Cannon, M., Roche, R.A., 2013. Reduced P300 amplitude during retrieval on a spatial working memory task in a community sample of adolescents who report psychotic symptoms. *BMC Psychiatry* 13, 125. <https://doi.org/10.1186/1471-244X-13-125>.
- Rottschy, C., Langner, R., Dogan, I., Reetz, K., Laird, A.R., Schulz, J.B., Fox, P.T., Eickhoff, S.B., 2012. Modelling neural correlates of working memory: a coordinate-based meta-analysis. *NeuroImage* 60, 830–846. <https://doi.org/10.1016/j.neuroimage.2011.11.050>.
- Roux, F., Uhlhaas, P.J., 2014. Working memory and neural oscillations: alpha–gamma versus theta–gamma codes for distinct WM information? *Trends Cogn. Sci.* 18, 16–25. <https://doi.org/10.1016/j.tics.2013.10.010>.
- Roux, F., Wibral, M., Mohr, H.M., Singer, W., Uhlhaas, P.J., 2012. Gamma-band activity in human prefrontal cortex codes for the number of relevant items maintained in working memory. *J. Neurosci.* 32, 12411–12420. <https://doi.org/10.1523/JNEUROSCI.0421-12.2012>.
- Sammer, G., Blecker, C., Gebhardt, H., Bischoff, M., Stark, R., Morgen, K., Vaitl, D., 2007. Relationship between regional hemodynamic activity and simultaneously recorded EEG–theta associated with mental arithmetic-induced workload. *Hum. Brain Mapp.* 28, 793–803. <https://doi.org/10.1002/hbm.20309>.

- Samu, D., Campbell, K.L., Tsvetanov, K.A., Shafto, M.A., Tyler, L.K., 2017. Preserved cognitive functions with age are determined by domain-dependent shifts in network responsiveness. *Nat. Commun.* 8, 14743. <https://doi.org/10.1038/ncomms14743>.
- Sauseng, P., Klimesch, W., Heise, K.F., Gruber, W.R., Holz, E., Karim, A.A., Glennon, M., Gerloff, C., Birbaumer, N., Hummel, F.C., 2009. Brain oscillatory substrates of visual short-term memory capacity. *Curr. Biol.* 19, 1846–1852. <https://doi.org/10.1016/j.cub.2009.08.062>.
- Sprague, T.C., Ester, E.F., Serences, J.T., 2014. Reconstructions of information in visual spatial working memory degrade with memory load. *Curr. Biol.* 24, 2174–2180. <https://doi.org/10.1016/j.cub.2014.07.066>.
- Sreenivasan, K.K., Curtis, C.E., D'Esposito, M., 2014a. Revisiting the role of persistent neural activity during working memory. *Trends Cogn. Sci.* 18, 82–89. <https://doi.org/10.1016/j.tics.2013.12.001>.
- Sreenivasan, K.K., Vytlačil, J., D'Esposito, M., 2014b. Distributed and dynamic storage of working memory stimulus information in extrastriate cortex. *J. Cogn. Neurosci.* 26, 1141–1153. [https://doi.org/10.1162/jocn\\_a\\_00556](https://doi.org/10.1162/jocn_a_00556).
- Sternberg, S., 1966. High-speed scanning in human memory. *Science* 153, 652–654. <https://doi.org/10.1126/science.153.3736.652>.
- Stevens, A.A., Tappon, S.C., Garg, A., Fair, D.A., 2012. Functional brain network modularity captures inter- and intra-individual variation in working memory capacity. *PLoS One* 7, e30468. <https://doi.org/10.1371/journal.pone.0030468>.
- Todd, J.J., Marois, R., 2004. Capacity limit of visual short-term memory in human posterior parietal cortex. *Nature* 428, 751–754. <https://doi.org/10.1038/nature02466>.
- Tong, S., Thakor, N.V., 2009. *Quantitative EEG Analysis Methods and Clinical Applications*. Artech House.
- Uddin, L.Q., Clare Kelly, A.M., Biswal, B.B., Castellanos, F.X., Milham, M.P., 2009. Functional connectivity of default mode network components: correlation, anticorrelation, and causality. *Hum. Brain Mapp.* 30. <https://doi.org/10.1002/hbm.20531>.
- Unsworth, N., Fukuda, K., Awh, E., Vogel, E.K., 2014. Working memory and fluid intelligence: capacity, attention control, and secondary memory retrieval. *Cogn. Psychol.* 71, 1–26. <https://doi.org/10.1016/j.cogpsych.2014.01.003>.
- Veltman, D.J., Rombouts, S.A.R.B., Dolan, R.J., 2003. Maintenance versus manipulation in verbal working memory revisited: an fMRI study. *NeuroImage* 18, 247–256. [https://doi.org/10.1016/S1053-8119\(02\)00049-6](https://doi.org/10.1016/S1053-8119(02)00049-6).
- Vermeij, A., van Beek, A.H.E.A., Reijs, B.L.R., Claassen, J.A.H.R., Kessels, R.P.C., 2014. An exploratory study of the effects of spatial working-memory load on prefrontal activation in low- and high-performing elderly. *Front. Aging Neurosci.* 6, 303. <https://doi.org/10.3389/fnagi.2014.00303>.
- Vogel, E.K., Machizawa, M.G., 2004. Neural activity predicts individual differences in visual working memory capacity. *Nature* 428, 748–751. <https://doi.org/10.1038/nature02447>.
- Vogel, E.K., McCollough, A.W., Machizawa, M.G., 2005. Neural measures reveal individual differences in controlling access to working memory. *Nature* 438, 500. <https://doi.org/10.1038/nature04171>.
- Wang, C., Ong, J.L., Patanaik, A., Zhou, J., Chee, M.W.L., 2016. Spontaneous eyelid closures link vigilance fluctuation with fMRI dynamic connectivity states. *Proc. Natl. Acad. Sci. U. S. A.* 113, 9653–9658. <https://doi.org/10.1073/pnas.1523980113>.
- Xie, Y., Feng, Z., Xu, Y., Bian, C., Li, M., 2016. The different oscillation patterns of alpha band in the early and later stages of working memory maintenance. *Neurosci. Lett.* 633, 220–226. <https://doi.org/10.1016/j.neulet.2016.09.047>.
- Zanto, T.P., Gazzaley, A., 2009. Neural suppression of irrelevant information underlies optimal working memory performance. *J. Neurosci. Off. J. Soc. Neurosci.* 29, 3059–3066. <https://doi.org/10.1523/JNEUROSCI.4621-08.2009>.
- Zhang, Q., Zhao, X., Zhu, C., Yang, X., Yao, L., 2015. Cortical activities of single-trial P300 amplitudes modulated by memory load using simultaneous EEG-fMRI, p. 94170L–94170L–6. <https://doi.org/10.1117/12.2080983>.
- Zhou, L., Thomas, R.D., 2015. Principal component analysis of the memory load effect in a change detection task. *Vis. Res.* 110 (Part A), 1–6. <https://doi.org/10.1016/j.visres.2015.01.028>.